A LETTERS JOURNAL EXPLORING THE FRONTIERS OF PHYSICS

OFFPRINT

Non-uniqueness of steady free-surface flow at critical Froude number

Benjamin J. Binder, Mark G. Blyth and Sanjeeva Balasuriya

EPL, **105** (2014) 44003

A Letters Journal Exploring the Frontiers of Physics

February 2014

EPL, **105** (2014) 44003
doi: 10.1209/0295-5075/105/44003

www.epljournal.org

Non-uniqueness of steady free-surface flow at critical Froude number

Benjamin J. Binder[1], Mark G. Blyth[2] and Sanjeeva Balasuriya[1]

[1] *School of Mathematical Sciences, University of Adelaide - Adelaide, Australia*
[2] *School of Mathematics, University of East Anglia - Norwich, UK*

received 5 December 2013; accepted in final form 12 February 2014
published online 4 March 2014

PACS 47.85.Dh – Applied fluid mechanics: Hydrodynamics, hydraulics, hydrostatics
PACS 47.35.-i – Hydrodynamic waves
PACS 47.15.K- – Inviscid laminar flows

Abstract – Free-surface flow past a disturbance at critical Froude number is commonly found to be unsteady with complex wave patterns both upstream and downstream of the disturbance. Such flows can be undesirable as the waves that are generated can have a negative impact in applications including the erosion of waterway banks and energy loss through wave drag on a ship. This motivates us to develop a new approach to obtain steady solutions at critical Froude number that are wave free in the far field. Under the assumption of two-dimensional, irrotational, incompressible fluid flow, we show that both weakly and fully nonlinear solutions to the problem are non-unique. A range of qualitatively different types of numerical solutions and analytical approximations are discovered, for example for flow over a corrugated channel bottom.

Introduction. – The study of steady two-dimensional gravity waves in finite depth channels has a rich and long history [1–11], which has continued to attract attention in more recent years [12–21]. A physical motivation for considering these flow problems is the well-known phenomenon where surface waves occur both upstream and downstream of a disturbance (*e.g.* ship or obstacle) that is moving at *critical speed* (fig. 1). Both experimental observations and theoretical predictions have shown that critical flows are in general unsteady with solitons [22] being radiated ahead of the steadily moving disturbance [17,19,23–30]. Unsteady critical flows provide interesting and complex wave patterns to investigate, but from a practical viewpoint the waves generated are undesirable for a number of reasons.

One reason is that the wash or wake generated by disturbances moving close to or at critical speed can damage both the integrity of waterway banks, leading to erosion and leaking, and the delicate eco-systems that live alongside them [31–34]. Another reason is that the energy lost in these surface waves is an important component of the overall drag on the disturbance [5,6,35–37]. This provides us with the incentive to develop a general approach to obtain steady critical flows [15,18,19,26,38], with no waves in the far field both upstream and downstream of the disturbance [26,38]. In particular, we demonstrate that steady critical flows are not unique —a fundamental result that, to the best of our knowledge, has not been previously reported in the vast amount of literature on this subject.

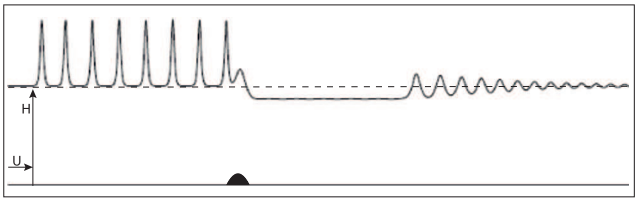

Fig. 1: Sketch of unsteady flow past a submerged obstacle moving at critical speed $U = \sqrt{gH}$ in an otherwise quiescent fluid. A frame of reference has been taken with the steadily moving obstacle. Typically, solitons are periodically generated upstream of the bump. Downstream of the obstacle there is a uniform depression and a wake that propagates downstream.

We assume the steady two-dimensional irrotational channel flow of an incompressible fluid. In a frame of reference moving with the disturbance the parameter that characterises the flow is the Froude number,

$$F = \frac{U}{\sqrt{gH}}, \tag{1}$$

where U and H are the uniform velocity and depth in the far field upstream, and g is the acceleration due to gravity. Equation (1) is the ratio of the uniform flow speed to the speed of small-amplitude (non-dispersive) waves in shallow water. The flow is supercritical upstream when $F > 1$, and subcritical upstream when $F < 1$. We define the flow to be critical when $F = F_d = 1$, where F_d is the Froude number in the far field downstream, but note that some authors define critical flow to mean $F < 1$ and $F_d > 1$ [9,12]. A hydraulic fall occurs when there is uniform subcritical flow upstream $F < 1$ and supercritical flow downstream $F_d > 1$.

In this letter we examine the existence and non-uniqueness of solutions for critical steady flows when $F = 1$ (and implicitly $F_d = 1$). Analytic and numerical solutions to a weakly nonlinear flow approximation [12,14,18,39,40] and fully nonlinear solutions to Euler's equations of motion, obtained by numerically solving a boundary integral equation [35,40–44], are found. The weakly and fully nonlinear results are illustrated respectively by solid and broken curves in our figures.

The success in obtaining solutions to both the weakly and fully nonlinear problems can be attributed to a common approach in methodology. The first stage in this general approach is to prescribe the boundary or interface between the air and water, called the free surface, and find the disturbance or forcing inversely [20,26,38]. We call this the inverse problem and it establishes the existence of at least one steady solution at critical Froude number. The second stage in the method is to prescribe the forcing (found using the inverse method in stage 1) and allow the free surface to come as part of the solution. This we call the forward problem and it is the usual approach taken in studies on free-surface flow problems (see references). Using parameter continuation methods for the forward problem, a second solution can sometimes be found.

Although we present solutions to both the weakly and fully nonlinear problems, we only give mathematical details of the weakly nonlinear problem, as it serves to better illustrate the key findings of this work. The formulation and computational procedures involved in the nonlinear problem can be found in [38].

To model the weakly nonlinear problem we use the forced Korteweg-de Vries (KdV) equation [39].

Forced KdV equation. – The (integrated) steady forced KdV equation [10,12,19,26,39,45–49], re-expressed in terms of dimensionless variables with only one characteristic length scale H, the constant depth in the far field [14,15], is

$$\eta_{xx}(x) + \frac{9}{2}\eta^2(x) - 6(F-1)\eta(x) = -3\sigma(x), \qquad (2)$$

where x measures distance in the streamwise direction. For a prescribed forcing, $\sigma(x)$, solutions of eq. (2) provide the free-surface elevation $\eta(x)$ above the unit level (in dimensionless terms) in the far field. Formally, if we set $\epsilon = \max|\sigma(x)|$, then eq. (2) is valid for $\epsilon \ll 1$, $\eta = O(\epsilon^{1/2})$ and $|1 - F| = O(\epsilon^{1/2})$.

The forcing σ can represent either a distribution of pressure on the free surface or a non-trivial (*i.e.* non flat) channel bottom topography [14,26,30,50]. Physically, a distribution of pressure can model the normal stress on the free surface generated by a moving ship [23,24,28,35,36,50] or the Maxwell stress due to a charged electrode [40], while changes in the channel bottom topography have a more obvious application in modelling flow over submerged obstacles [12,13,15,17,20,26,51].

We begin our investigation with the forward problem, taking a localised forcing with compact support given by

$$\sigma(x) = \alpha\delta(x), \qquad (3)$$

where $\delta(x)$ is the Dirac delta function.

The forward problem. – The existence of steady solutions for localised forcing with compact support can be explained with an analysis in the weakly nonlinear phase plane of the problem [12,14,18,40], by replacing the model eqs. (2) and (3) with

$$\eta_{xx}(x) + \frac{9}{2}\eta^2(x) - 6(F-1)\eta(x) = 0 \qquad (4)$$

for $x \neq 0$, and

$$\eta_x(0^+) - \eta_x(0^-) = -3\alpha. \qquad (5)$$

Equation (4) is a two-dimensional nonlinear autonomous dynamical system, and integrating (4) gives the solution trajectories

$$\eta_x^2(x) = 6(F-1)\eta^2(x) - 3\eta^3(x) + \mathcal{C} \qquad (6)$$

in the phase plane (η, η_x). The constant of integration, $\mathcal{C}$, in eq. (6) determines the solution trajectory in the phase plane, and the equilibrium points are classified in the caption of fig. 2. The vertical jump condition, eq. (5), with amplitude of forcing α, provides a way to jump discontinuously between the trajectories.

Consistent with the work of others [19,25,52], we can define, using eqs. (5), (6), a transcritical range valid for $\alpha > 0$, in which no steady solutions exist,

$$1 - \left(\frac{9\alpha}{4\sqrt{2}}\right)^{2/3} < F < 1 + \left(\frac{9\alpha}{8\sqrt{2}}\right)^{2/3}. \qquad (7)$$

The lower bound of the transcritical range occurs when the period of the cnodial waves, typically found in subcritical flow, approaches infinity, and in this case there is a hydraulic fall. This is illustrated in the phase plane diagram, fig. 2(a), by a vertical jump from the null solution to the homclinic solution trajectory. The upper bound corresponds to the turning point in the saddle-node bifurcation diagrams [8,25,40], $\eta(0)$ *vs.* F, for supercritical flow. This is illustrated in the phase plane diagram, fig. 2(b), with a

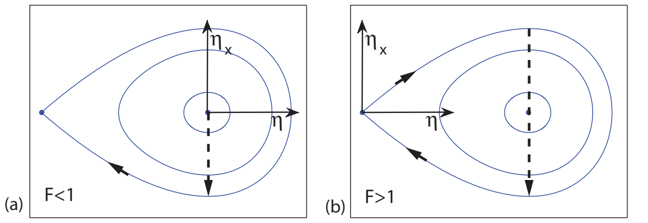

Fig. 2: (Colour on-line) Existence of steady solutions in the phase plane (η, η_x) for a localised forcing with compact support and amplitude of forcing $\alpha > 0$. (a) Subcritical flow, $F < 1$, with a saddle at $(4/3(F-1), 0)$ and a centre at (0,0). The homoclinic orbit is for a value of $\mathcal{C} = \frac{32}{9}(1-F)^3$ in eq. (6). The length of the broken arrow illustrates the maximum amplitude of forcing, $\alpha = \frac{4\sqrt{2}}{9}(1-F)^{3/2}$. (b) Supercritical flow, $F > 1$, with a saddle at (0,0) and a centre at $(4/3(F-1), 0)$. The homoclinic orbit is for a value of $\mathcal{C} = 0$ in eq. (6). The length of the broken arrow illustrates the maximum amplitude of forcing, $\alpha = \frac{8\sqrt{2}}{9}(F-1)^{3/2}$.

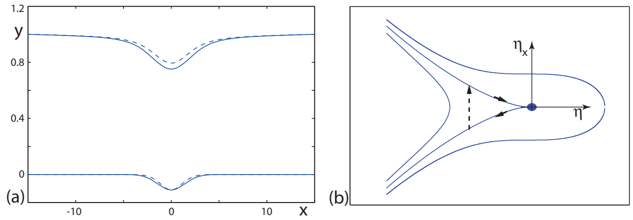

Fig. 3: (Colour on-line) Steady solution at critical Froude number for localised forcing. (a) Free-surface solutions to the forward problem with $F = 1$ for prescribed forcing, $\alpha = -0.60$ and $\beta = 0.50$. The solid and broken curves are for the weakly nonlinear and nonlinear values, respectively. (b) Sketch of solution in the weakly nonlinear phase plane (η, η_x).

vertical jump between the maximum and minimum values in η_x for the homclinic solution trajectory. Within this transcritical range the flow in general is intrinsically unsteady, and can exhibit the complex wave patterns shown in fig. 1.

When $\alpha < 0$, there are no steady solutions if F lies in the subcritical range

$$1 - \left(\frac{9|\alpha|}{4\sqrt{2}}\right)^{2/3} < F < 1. \tag{8}$$

However, steady solutions may be constructed for localised point forcing if $F \geq 1$ and $\alpha < 0$. This is illustrated for critical flow ($F = 1$) in fig. 3(b). Here there is only one equilibrium point, which is located at the origin, and any bounded solution must start and end its journey through the phase plane at this point in order to fulfil the far-field conditions. This equilibrium point is degenerate (in contrast to the subcritical and supercritical regimes) and thus straightforward linearisation techniques for analysis of nearby behaviour fail. We see from fig. 3(b) that it is impossible to make a downwards vertical jump (corresponding to a positive amplitude of forcing, $\alpha > 0$) in the phase plane to create a bounded solution. However a bounded solution can be constructed by making an upwards vertical jump, with $\alpha < 0$, as is illustrated by the broken line in the figure. A similar construction in the phase plane for supercritical flow, $F > 1$, is permissible by following a similar path out of the saddle in the left-hand plane of fig. 2(b) (not shown).

For the critical flow case, $F = 1$, we computed numerical solutions to both the weakly and fully nonlinear (forward) problems by approximating the forcing $\sigma(x) = \alpha\delta(x)$ with

$$\sigma(x) = \frac{\alpha\beta}{\sqrt{\pi}} \exp\left[-(\beta x)^2\right], \tag{9}$$

for constants α and β, noting that

$$\sigma(x) \to \alpha\delta(x) \quad \text{as} \quad \beta \to \infty. \tag{10}$$

As predicted by the phase plane analysis, we only find one solution for a given value of α, even when $\beta = O(1)$. Typical wave profiles are shown in fig. 3(a).

We are not the first to compute steady flow at critical Froude number [15,17,19,26,40], but to our knowledge we are the first to recognise that in the case of localised forcing with compact support the solution is unique, as has been demonstrated by our phase plane analysis. Next we broaden the range of critical solutions when $F = 1$ by relaxing the assumption of a point forcing in our phase plane analysis. In this case the resulting dynamical system to be studied is non-autonomous and the previous phase plane analysis is not applicable.

The inverse problem. – One solution to eq. (2) can be found by prescribing the function $\eta(x)$ which satisfies the far-field uniform flow conditions $\eta_{xx}(x) \to 0$ $\eta_x(x) \to 0$, $\eta(x) \to 0$, as $x \to \pm\infty$. The forcing $\sigma(x)$ is then determined inversely from eq. (2), with $\sigma(x) \to 0$ as $x \to \pm\infty$. For example,

$$\begin{aligned}\eta(x) \;=\; & a_1 \exp\left[-b^2(x-p)^2\right] + a_2 \exp\left[-b^2(x+p)^2\right] \\ & + c \tanh\left[b(x-q)\right] - c \tanh\left[b(x+q)\right],\end{aligned} \tag{11}$$

where a_1, a_2, b, c, p and q are chosen constants, is a suitable linear combination of candidate functions provided $b > 0$.

The solid upper and lower curves in fig. 4(a) is an inverse (weakly nonlinear) solution, with only the non-zero parameters of eq. (11) being reported in the figure caption. A similar approach is used in the nonlinear solutions, although the forcing has to be solved for numerically [38]. The close-up plot shown in fig. 4(b) illustrates the difference between the weakly and fully nonlinear solutions for the forcing.

The idea now is to obtain a second forward solution for $\eta(x)$ with this inversely found forcing. In both the weakly and fully nonlinear problems this is done numerically using continuation methods —see the middle curves (solid

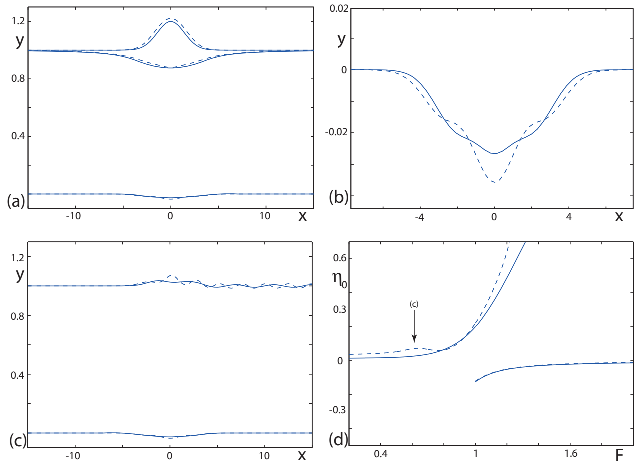

Fig. 4: (Colour on-line) Non-uniqueness of solutions at critical Froude number. The solid and broken curves are for the weakly nonlinear and nonlinear values, respectively. (a) Flow with $F = 1$. The two bottom curves are solutions for the forcing found using the inverse method for a prescribed free-surface shape (top two curves), $a_1 = 0.20$ and $b = 0.50$. The two middle curves are forward solutions for the free surface with prescribed forcing (bottom two curves). (b) Close-up of the inversely found forcing in (a). (c) Free-surface profiles (top two curves) with $F = 0.60$ for prescribed forcing (bottom two curves). (d) Plot of $\eta(0) = \eta_0$ *vs.* F, for the inversely found forcing.

and broken) in fig. 4(a). For the inversely found forcing, the bifurcation diagram of fig. 4(d) illustrates that the solution branches are disconnected at $F = 1$. The solutions on the top and bottom branch (fig. 4(d)) with $F = F_d > 1$ look qualitatively similar to the upper and lower free-surface curves in fig. 4(a), respectively. Solutions on the top branch (fig. 4(d)) with $F < 1$ are characterised with a train of periodic waves on the free surface and uniform flow as $x \to -\infty$ as is shown in fig. 4(c). The amplitude and wavelength of the periodic waves are independent of where the domain is truncated (provided the truncated domain is large enough), and the solutions are therefore unique. The subcritical solutions of fig. 4(c) correspond to the arrow seen in fig. 4(d).

Using our inverse-forward-approach, a wide range of other qualitatively different non-unique solutions with $F = 1$ are shown in fig. 5(ai)–(aiii).

Corrugated channel bottom topography. – To conclude our study we consider a trapped cosine wave-train on the free surface (top curves, fig. 5(bi)–(biii)) prescribed by

$$\eta(x) = A\cos[Dx]\left(\frac{1}{2}+\frac{1}{2}\tanh[Q-x]\right) \times\left(\frac{1}{2}+\frac{1}{2}\tanh[Q+x]\right), \qquad (12)$$

where A, D, and Q are chosen constants. Inverse solutions for the forcing are shown by the bottom curves

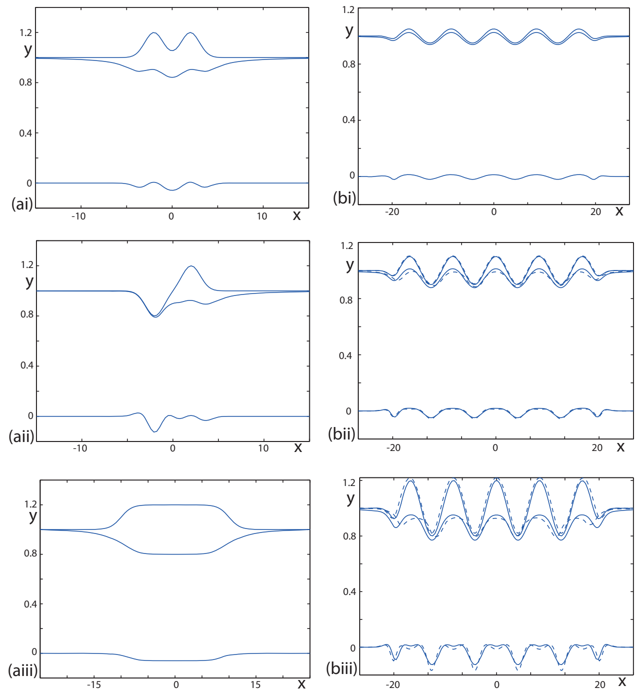

Fig. 5: (Colour on-line) Further examples of non-uniqueness at critical Froude number, $F = 1$. (ai)–(aiii): qualitatively different weakly nonlinear solutions. (ai) $a_1 = a_2 = 0.20$, $p = 2.0$ and $b = 0.70$. (aii) $a_1 = -0.2$, $a_2 = 0.20$, $p = 2.0$ and $b = 0.70$. (aiii) $c = -0.10$, $q = 10.0$ and $b = 0.50$. (bi)–(biii): weakly nonlinear and nonlinear solutions for a corrugated channel bottom, $Q = 15$ and $D = 1.0$. The solid and broken curves are for the weakly nonlinear and nonlinear values, respectively. (bi) $A = 0.05$, (bii) $A = 0.1$, (biii) $A = 0.2$.

in fig. 5(bi)–(biii), for increasing amplitude, A, of the free-surface cosine waves. Forward solutions with the inversely found forcing are then computed (middle curves of fig. 5(bi)–(biii)), and demonstrate the non-uniqueness of solutions at the critical value of the Froude number.

We see that the two qualitatively different types of wave-trains on the free surface converge when $A \ll 1$, and the nonlinear solutions are visually indistinguishable (not shown) from the weakly nonlinear solutions (fig. 5(bi)). It is also easy to show using eqs. (2) and (12) that the trapped wave-train of the forcing is given by

$$\sigma(x) \approx \frac{AD^2}{3}\cos[Dx] - \frac{3A^2}{2}\cos^2[Dx] \quad \text{for} \quad |x| < Q, \qquad (13)$$

where the approximate form represents the forcing which is formally obtained in the limit $Q \to \infty$. For small-amplitude forcing, the free-surface deformation is approximately $3/D^2$ of the forcing amplitude, implying that the surface response is amplified (according to a square law) for longer-wavelength forcing.

Closing remarks. – We have demonstrated the non-uniqueness of solutions at the critical value of the Froude number, and have discovered many new qualitatively different types of solutions. The non-uniqueness for non-local forcing arises from the fact that the phase plane in fig. 3(b) needs to have an appended coordinate x out of the page in this non-autonomous case, thereby allowing for the possibility of several different solutions which asymptote to the x-axis as $x \to \pm\infty$. Our approach can easily be extended to a general surface by replacing eqs. (11) or (12) with a different specification, calculating the required forcing using the inverse approach, and then performing numerical investigations.

We remark that in a more general bottom topography problem, the free-surface profile does not necessarily flatten out as $x \to \pm\infty$. This hinders most numerical schemes, while also providing theoretical difficulties as the system is no longer uniform in the far field (both upstream and downstream). As a result, there is little current insight into such solutions. In a forthcoming paper, we will provide a theoretical framework building on non-autonomous dynamical systems ideas [53–55] which establishes the existence and uniqueness of solutions when $\sigma(x)$ is non-decaying but small, and which, moreover provides explicit analytical approximations for such solutions.

REFERENCES

[1] Lamb H., *Hydrodynamics* (Cambridge University Press) 1879.
[2] Havelock T. H., *Proc. R. Lond. A*, **93** (1917) 520.
[3] Havelock T. H., *Proc. R. Lond. A*, **100** (1922) 499.
[4] Lighthill M. J., *Waves in Fluids* (Cambridge University Press) 1978.
[5] Forbes L. K., *J. Eng. Math.*, **15** (1981) 287.
[6] Forbes L. K., *J. Eng. Math.*, **16** (1982) 171.
[7] Forbes L. K. and Schwartz L. W., *J. Fluid Mech.*, **114** (1982) 299.
[8] Vanden-Broeck J.-M., *Phys. Fluids*, **30** (1987) 2315.
[9] Forbes L. K., *J. Eng. Math.*, **22** (1988) 3.
[10] Grimshaw R. H. and Smyth N., *J. Fluid Mech.*, **169** (1986) 429.
[11] Dias F. and Vanden-Broeck J.-M., *J. Fluid Mech.*, **206** (1989) 155.
[12] Dias F. and Vanden-Broeck J.-M., *J. Eng. Math.*, **42** (2002) 291.
[13] Dias F. and Vanden-Broeck J.-M., *J. Fluid Mech.*, **509** (2004) 93.
[14] Binder B. J., Vanden-Broeck J.-M. and Dias F., *Chaos*, **15** (2005) 037106.
[15] Binder B. J., Dias F. and Vanden-Broeck J.-M., *Theor. Comput. Fluid Dyn.*, **20** (2006) 124.
[16] Grimshaw R., Maleewong M. and Asavanant J., *Phys. Fluids*, **21** (2009) 082101.
[17] Ee B. K., Grimshaw R., Zhang D.-H. and Chow K. W., *Phys. Fluids*, **22** (2010) 056602.
[18] Binder B. J. and Vanden-Broeck J.-M., *Phys Rev. E.*, **84** (2011) 016302.
[19] Grimshaw R., *ANZIAM J.*, **52** (2011) 1.
[20] Chardard F., Dias F., Nguyen H. Y. and Vanden-Broeck J.-M., *J. Eng. Math.*, **70** (2011) 175.
[21] Grimshaw R. and Maleewong M., *Phys. Fluids.*, **25** (2013) 076605.
[22] Zabusky N. J. and Galvin C. J., *J. Fluid Mech.*, **47** (1971) 811.
[23] Mei C. C., *J. Fluid Mech.*, **162** (1986) 53.
[24] Lee S.-J., Yates G. T. and Wu T. Y., *J. Fluid Mech.*, **199** (1989) 569.
[25] Miles J. W., *J. Fluid Mech.*, **162** (1986) 489.
[26] Wu T. Y.-T., *J. Fluid Mech.*, **184** (1987) 75.
[27] Thews J. G. and Landweber L., *The influence of shallow water on the resistance of a cruiser model*, US Experimental Model Basin, Washington, DC, Report 408 (1934).
[28] Wu D. M. and Wu T. Y., *Three-dimensional nonlinear long waves due to moving surface pressure*, *Proceedings of the 14th Symposium Naval Hydrodynamics* (National Academy Press, Washington, DC) 1982.
[29] Huang D. B., Sibul O. J., Webster W. C., Wehausen J. V., Wu D. M. and Wu T. Y., *Ships moving in the transcritical range*, *Proceedings of the Conference on Behaviour of Ships in Restricted Waters, Varna, Bulgaria, 1982*, pp. 26-1–26-10.
[30] Erktekin R. C., Webster W. C. and Wehausen J. V., *J. Fluid Mech.*, **169** (1986) 275.
[31] Ellis J. T., Sherman D. J., Bauer B. O. and Hart J., *J. Coast. Res.*, **36** (2002) 256.
[32] Bishop M. J., *Environ. Manage.*, **34** (2004) 140.
[33] Bishop M. J. and Chapman M. G., *Estuarine Coastal Shelf Sci.*, **61** (2004) 613.
[34] Nanson G. C., Von Krusenstierna A. and Bryant E. A., *Regulated rivers: Research and Management*, **9** (1994) 1.
[35] Binder B. J., *Phys. Fluids.*, **22** (2010) 012104.
[36] Farrow D. E. and Tuck E. O., *J. Aust. Math. Soc. Ser. B*, **36** (1995) 427.
[37] McCue S. W. and Stump D., *Q. J. Mech. Appl. Math.*, **53** (2000) 629.
[38] Binder B. J., Blyth M. and McCue S. W., *IMA J. Appl. Math.*, **78** (2013) 685.
[39] Korteweg D. J. and De Vries G., *Philos Mag.*, **5** (1895) 422.
[40] Binder B. J. and Blyth M. G., *Phys. Fluids.*, **24** (2012) 102112.
[41] Levi-Civita T., *Math. Ann.*, **93** (1925) 264.
[42] Vanden-Broeck J.-M., *J. Fluid Mech.*, **330** (1996) 339.
[43] Binder B. J. and Vanden-Broeck J.-M., *J. Fluid Mech.*, **576** (2007) 475.
[44] Binder B. J., Vanden-Broeck J.-M. and Dias F., *IMA J. Appl. Math.*, **73** (2008) 254.
[45] Akylas T. R., *J. Fluid Mech.*, **141** (1984) 455.
[46] Shen S. S.-P., *J. Appl. Math. Phys.*, **42** (1991) 122.
[47] Camassa R. and Wu T. Y., *Philos Trans. R. Soc. London, Ser. A*, **337** (1991) 429.
[48] Gong L. and Shen S. S.-P., *SIAM J. Appl. Math.*, **54** (1994) 1268.
[49] Shen S. S.-P., *Q. J. Appl. Math.*, **53** (1995) 701.
[50] Binder B. J. and Vanden-Broeck J-M., *Eur. J. Appl. Math.*, **16** (2005) 601.
[51] Pratt L. J., *Geophys. Astrophys. Fluid Dyn.*, **24** (1984) 63.
[52] Cole S. L., *Q. J. Appl. Maths.*, **41** (1983) 301–309.

[53] Balasuriya S., *SIAM J. Appl. Dyn. Syst.*, **10** (2011) 1100.

[54] Balasuriya S., *Nonautonomous flows as open dynamical systems: characterising escape rates and time-varying boundaries*, in *Ergodic Theory, Open Dynamics and Coherent Structures*, edited by Bahsoun W., Bose C. and Froyland G., *Springer Proceedings in Mathematics*, 2014, in print.

[55] Balasuriya S. and Padberg-Gehle K., *SIAM J. Appl. Math.*, **73** (2013) 1038.